Environmental Science Processes & Impacts

ROYAL SOCIETY OF CHEMISTRY

PAPER

Cite this: *Environ. Sci.: Processes Impacts*, 2021, **23**, 73

Emerging investigator series: entrapment of uranium–phosphorus nanocrystals inside root cells of *Tamarix* plants from a mine waste site†

Lucia Rodriguez-Freire, *[a] Cherie L. DeVore,[b] Eliane El Hayek,[c] Debora Berti, [d] Abdul-Mehdi S. Ali,[e] Juan S. Lezama Pacheco,[f] Johanna M. Blake, [cg] Michael N. Spilde,[e] Adrian J. Brearley,[e] Kateryna Artyushkova[h] and José M. Cerrato [b]

We investigated the mechanisms of uranium (U) uptake by *Tamarix* (salt cedars) growing along the Rio Paguate, which flows throughout the Jackpile mine near Pueblo de Laguna, New Mexico. *Tamarix* were selected for this study due to the detection of U in the roots and shoots of field collected plants (0.6–58.9 mg kg^{-1}), presenting an average bioconcentration factor greater than 1. Synchrotron-based micro X-ray fluorescence analyses of plant roots collected from the field indicate that the accumulation of U occurs in the cortex of the root. The mechanisms for U accumulation in the roots of *Tamarix* were further investigated in controlled-laboratory experiments where living roots of field plants were macerated for 24 h or 2 weeks in a solution containing 100 μM U. The U concentration in the solution decreased 36–59% after 24 h, and 49–65% in two weeks. Microscopic and spectroscopic analyses detected U precipitation in the root cell walls near the xylems of the roots, confirming the initial results from the field samples. High-resolution TEM was used to study the U fate inside the root cells, and needle-like U–P nanocrystals, with diameter <7 nm, were found entrapped inside vacuoles in cells. EXAFS shell-by-shell fitting suggest that U is associated with carbon functional groups. The preferable binding of U to the root cell walls may explain the U retention in the roots of *Tamarix*, followed by U–P crystal precipitation, and pinocytotic active transport and cellular entrapment. This process resulted in a limited translocation of U to the shoots in *Tamarix* plants. This study contributes to better understanding of the physicochemical mechanisms affecting the U uptake and accumulation by plants growing near contaminated sites.

Received 15th July 2020
Accepted 24th November 2020

DOI: 10.1039/d0em00306a

rsc.li/espi

Environmental significance statement

This work represents a unique investigation that integrates field and laboratory approaches to identify the mechanisms for U accumulation in invasive *Tamarix* plants extensively growing near an abandoned uranium mine waste site. Field-grown *Tamarix* plants accumulated U in their roots. *In vitro* experiments allowed us to study U interactions with cell walls or cell membranes in the plant roots. Localized U precipitation lead to entrapment inside the cells as needle-like uranium–phosphorus nanocrystals. This research highlights the importance of local plants controlling U transport near contaminated sites, which can inform exposure assessment and phytoremediation strategies.

[a]*Department of Civil and Environmental Engineering, New Jersey Institute of Technology, Newark, New Jersey 07102, USA. E-mail: lrfreire@njit.edu; Fax: +1 973 596-5790; Tel: +1 973 596-2448*

[b]*Department of Civil Engineering, MSC01 1070, University of New Mexico, Albuquerque, New Mexico 87131, USA*

[c]*Department of Chemistry, MSC03 2060, University of New Mexico, Albuquerque, New Mexico 87131, USA*

[d]*Oceanography Department, Texas A&M University, College Station, Texas 77845, USA*

[e]*Department of Earth and Planetary Sciences, MSC03 2040, University of New Mexico, Albuquerque, New Mexico 87131, USA*

[f]*Department of Environmental Earth System Science, Stanford University, Stanford, California 94305, USA*

[g]*U.S. Geological Survey, 6700 Edith Blvd NE, Albuquerque, New Mexico 87113, USA*

[h]*Department of Chemical and Biological Engineering, MSC01 1120, University of New Mexico, Albuquerque, New Mexico 87131, USA*

† Electronic supplementary information (ESI) available. See DOI: 10.1039/d0em00306a

1. Introduction

Extensive uranium (U) mining took place in the 1950's and peaked in the late 1970's, producing more than 40 billion pounds of U in the United States alone.[1] Over 15 000 abandoned mines are a legacy of these activities,[2] leaving approximately 199 billion kilograms of U-containing residues near these sites.[3] Uranium concentration in mine waste solids can be as high as 1% (or 10 000 mg kg^{-1}),[4] compared to the average crustal earth concentration of 3 mg kg^{-1}.[5] Furthermore, radionuclides from uranium decay (daughters) might be present in mine wastes, accounting for up to 85% of the original radioactivity.[6] Hence, these abandoned U mine wastes represent a concern for populations living near them. In the United States, about 75% of the

abandoned mines are in federal and tribal lands in the states of Colorado, Utah, New Mexico, Arizona, and Wyoming.[2,7,8] Understanding the mechanisms for U transformations that affect the transport and/or immobilization in the environment is essential to identify potential routes for human exposure and remediation.

Biogeochemical processes influence mineralogical and chemical transformations that affect the transport of U and other co-occurring elements in the environment. Extensive research has investigated the effect of biogeochemical processes on the transport of U in subsurface and surface environments.[9,10] Uranium in waters adjacent to mine wastes exposed to oxidizing conditions is mostly present as U(VI).[11] However, the presence of reduced solid forms of U(IV) in surface oxidizing environments has also been reported.[4,11–13] Physical, chemical and biological processes determine whether U is retained in sediments or dissolved in water systems. U mobilization and bioavailability is promoted through its complexation with aqueous ligands[14–16] and dissolved organic matter;[17–19] while U immobilization is controlled through precipitation[20–22] and sorption reactions with soil minerals[23–26] and soil organic matter.[27] In addition, redox transformations of U play an important role in U solubility.[28,29] Oxidized, U(VI) (uranyl cation, $U(VI)O_2^{2+}$) is readily soluble, while its reduced form, U(IV) (uraninite, $U(IV)O_2$) is highly insoluble. U reductive precipitation to uraninite can be catalyzed by chemical processes[30–32] and by biologically-mediated reactions,[29,33,34] in which U(VI) is used as terminal electron acceptor by metal reducing bacteria to support metabolic growth.[35–37] However, uraninite is only stable under reducing environments, and U(IV) is readily oxidized to U(VI) under aerobic conditions or in the presence of alternative terminal electron acceptors, such as iron(III)[38,39] and nitrate.[40,41] Processes leading to higher U mobility will increase the bioavailability of U to local biota,[42–44] including phytoaccumulation of U by local plants.[45–47] Although U is considered a unique chemotoxic and radiotoxic element, the chemical toxicity of uranium generally represents greater environmental risks than its radiological toxicity because of the uranium isotope's long physical half-life (704 million years for U-235 or 4.5 billion years for U-238). Mathews *et al.*[96] have shown that U's chemical toxicity generally surpasses its radiological toxicity to the environment by evaluating the risks of chronic exposure to uranium in freshwater ecosystems. Ribera *et al.*[95] reported that the radiological toxicity of U becomes significant at concentrations considerably higher than those detected in the environment.

Uranium uptake by plants has been investigated from two major foci: (1) U accumulation in agricultural or harvesting plants with the potential risk for human exposure;[48,49] and (2) U phytoremediation of contaminated sites.[50–52] Uranium interaction with ligands is known to affect its bioavailability,[42–44] which impact metal reactivity and mobility. Wetlands can promote U immobilization through complexation with local ligands and organic matter.[53–56] Within plants, uranium complexation with carbonate or citric acid, enhances U accumulation and translocation to the shoot,[49,51] due to the transport of U from root-to-shoot as a U–carboxylate complex form;.[57,58] In contrast, if U is present as a soluble U(VI), the immobilization mainly occurs in the roots, most likely due to its complexation with phosphorus (P) and plant proteins.[57–59] Exposure to acidic pH (4–5) has been shown to enhance the accumulation of U from soil by plants, and promote the precipitation of crystalline uranyl phosphate in plant roots, while U accumulation has been shown to be partially inhibited at alkaline pH and result in the formation of an amorphous U–P mineral, which is an indication of the important role on U speciation on the U–cell interactions.[59] Additionally, the addition of soluble calcium (Ca^{2+}) amended as $CaHCO_3$ has shown to decrease U bioavailability and uptake by *Brassica juncea*.[60] However, existing studies on U accumulation in plants have mainly been conducted under controlled conditions, where the seeds are grown and exposed to U in laboratory settings. The mechanisms for U transport in native plants growing near abandoned uranium mines are poorly understood.

Our main research objective was to investigate the uptake and accumulation of U in the plants growing adjacent to the Rio Paguate after it flows through the Jackpile mine. The concentrations of U in mine waste solids from this site located in New Mexico can be as high as 9200 mg kg^{-1}.[4] The Rio Paguate flows through the mine and downstream to a wetland and reservoir. The Pueblo de Laguna is a Native American community with two villages (Paguate and Mesita) located less than 5 km from the mine depending on the river water for agriculture and livestock activites. The U concentration in the Paguate River water ranged from 35–770 μg L^{-1}, but the measured uranium concentration in the sediments was low (1–5 mg kg^{-1}).[4] Vegetation of the river bank consists in grasses, *Typha latifolia* (cattail), and *Salix* (dessert willows), but the invasive species *Tamarix* (Salt Cedars) dominate the landscape. *Tamarix* are phreatophytes, with extensive root systems as deep as 50 m, and can grow up to 4 m in a growing season.[61] *Tamarix* plants can last for 75–100 years, and they have replaced between 75–90% of the native vegetation in the Southwest since 1960.[61–63] For these reasons, the invasive *Tamarix* was selected as our study plant due to its abundance in this site, the extensive root systems, and fast growth rate, which can play an important role affecting the fate of U in the area. We used a combination of water chemistry, spectroscopic and microscopic analyses to quantify and analyze the accumulation and distribution of U in *Tamarix* plants collected from the field, and we used *in vitro* experiments to elucidate the mechanisms of interaction and accumulation of U in the roots, particularly the cortical tissue, where high concentrations of U could likely occur in the plant root system.[57,60,64] Insights from field and laboratory results in this study contribute to identify the bioavailability and plant uptake of U in the sediments of the riverbank of Rio Paguate and to evaluate the potential of *Tamarix* plants, the most abundant plant at the mine site, for U phytoaccumulation. This information is relevant to inform phytoremediation strategies and to better understand the biogeochemical interaction of U in the rhizosphere of native plants growing in the proximity of mine waste sites.

2. Materials and methods

2.1. Field study

Tamarix plants are invasive species in the Southwest of United States, and grow near the Rio Paguate. In order to assess the potential of U uptake by *Tamarix*. Samples were collected from the stream banks of Rio Paguate, as shown in the map presented in Fig. S1 in the ESI,† from the Jackpile mine to a wetland situated 5 km downstream from the mine (Table 1) at different times throughout a year, as a previous study has observed a correlation between U transport from the mine and the river flowrate.[4] *Tamarix* samples were collected using a clean shovel (rinse with 2% HNO_3, ethanol and deionized water) to a depth of 60 cm. The shovel was cleaned with water after every sample was collected to avoid cross-contamination. Plants were shaken in the field, to remove as much sediment as possible, and stored in a paper bag with rhizosphere soil until washed. Once the sample arrived in the laboratory, each plant was carefully transferred from paper bags to pre-cleaned clear plastic containers. Each plant was carefully separated into its roots and shoots parts. Plant parts were rinsed and triple washed with deionized water, with a final rinse using 18 MΩ water. The plant parts were then air-dried for 24 h, and then further dried in an oven at 65 °C for 3 h until thoroughly dry. Dried samples were ground using a coffee grinder, which was carefully cleaned between each sample type. A 1 g mass of dried plant was weighed and added to the digestion tube, and digested with 9 mL of ultra-high purity HNO_3 and 2 mL H_2O_2 for 60 min at 65 °C and then for an additional 60 min at 80 °C in a Digi prep MS SCP Science block digester. The digested samples were diluted using 18 MΩ water to 25 mL, and filtered through at 0.45 μm filter (25 mm PTFE membrane syringe filter) to remove any remaining particulate matter, and analyzed for total elemental concentrations using Inductively Coupled Plasma (ICP) coupled with a Mass Spectrometer (MS), ICP-MS.

Surface water and sediment data was presented in a previous study by Blake *et al.*[4] Briefly, surface water was collected in 250 mL polypropylene (PP) Nalgene bottles with zero head space when possible, filtered through 0.45 μm Whatman filters and then through 0.22 μm filters. Samples were acidified to pH < 2 with ultra-high purity HNO_3. Sediment samples were collected with a hand trowel (cleaned between each use with DI water) and placed in gallon plastic bags. Homogenized sediment samples (1 g) were digested using 2 mL ultra-high purity HNO_3 and 6 mL HCl and filtered through 0.45 μm filters. Water and sediment samples were analyzed for U using ICP-MS. Water pH ranged from 6.8 to 8.6. Sediment characterization with X-ray photoelectron spectroscopy (XPS) indicated the presence of mixed iron as 62–72% Fe(III) and 38–28% Fe(II) in the sediments, indication of an oxic surface environment.

2.2. *In vitro* experiments

The mechanisms for U accumulation in the roots were investigated using *in vitro* experiments, where fresh living root tissues from mature *Tamarix* plants collected from the field were exposed to high U concentrations. Mature plants differ from young plants in the water transport,[65] metal interaction,[66] and genetic expression.[67] Because of their long lifespan and local proliferation, mature plants are more relevant to this study, but their extensive and strong root systems complicate the transplantation from field to laboratory settings. Plant cuttings have been widely used as a method for vegetative propagation where the living cells in the root tissue (cortical parenchyma in particular) should remain alive and metabolically active.[68,69] *In vitro* experiments using root cuttings will allow investigating the cellular mechanisms for U interaction and accumulation in living root tissues. With this objective, washed and clean root samples (0.5–1 cm diameter) from the field were radially cut in approximately 5 mm thick pieces using a utility cutter, briefly rinsed with 2% HNO_3, ethanol, and 18 MΩ water. Three pieces of the roots were weighed and added to a 50 mL centrifuge tube. 25 mL of a solution containing 100 μM of U as uranyl acetate ($C_4H_6U{\cdot}2H_2O$, American Elements) and 0.2 M NaCl was mixed with the roots in six different tubes and incubated at room temperature in a rotational shaker, three of them were incubated for 24 h, and the remaining three were incubated for two weeks. Three additional tubes were incubated with only 0.2 M NaCl as blank controls for two weeks. The saline solution was used to help maintain optimal osmotic conditions for the living root tissues. The pH of the solution was adjusted to 7.0 using NaOH or HCl. At the end of the incubation period, the root samples were collected from the solution, gently rinsed with a solution containing only 0.2 M NaCl to remove any superficial U, and air-dried for 24 h. The root samples were analyzed using a variety of microscopic and spectroscopic techniques as indicated below. Liquid samples were also collected at the beginning and at the end of the incubation, and analyzed for total uranium concentrations in the ICP-MS.

2.3. Analytical techniques

Elemental composition of all samples was measured using Inductively Coupled Plasma (ICP) coupled with a Mass Spectrometer (MS), PerkinElmer NexION 300D (Dynamic Reaction Cell) with a detection limit of <0.5 μg L^{-1}. Chemical equilibrium modeling was conducted using MINEQL+ v4.6 [70] to gain further insights about relevant reactions for the *in vitro* experiments.

Scanning Transmission Electron Microscopy (STEM) was used to investigate the location of U accumulation in the roots. STEM analysis was performed using a JEOL 2010F FEGTEM/STEM operating at 200 kV. Root pieces from the *in vitro* experiment were air dried and coated with Au–Pd and placed on Cu TEM grids. High-angle annular dark-field (HAADF) images of the samples were obtained and then representative areas of the sample were studied using STEM X-ray mapping. An Oxford Instruments Aztec Energy Dispersive Spectroscopy (EDS) analysis system coupled to an $XMax^N$ 80 mm^2 EDS detector was used to obtained full spectral X-ray maps of the sample. After collection of the maps, EDS X-ray spectra for individual mineral phases were extracted from the data cube by drawing regions of interest around distinct mineral grains based on the HAADF images. This approach allows integration of X-ray counts from

Table 1 Acid digestion data of the salt cedar samples collected from the field

Location	Date[a]	N^b	Root[c] U (mg kg^{-1})	Stem U (mg kg^{-1})	Leaves U (mg kg^{-1})	Water data[d] (μg L^{-1})	Sediment data[d] (mg kg^{-1})	BF[e] (roots/sediment)	BF (stem/sediment)	TF[f]
Jackpile mine	Feb, 15	1	56	1.6	—	35	2.7 ± 0.2	20.4	0.6	0.03
	May, 15	3	25 ± 5	1.2 ± 0.5	7.3 ± 0.2	148	2.2 ± 0.05	11 ± 2	3.3 ± 0.1	0.29
	May, 15	3	18 ± 7	1.7 ± 2	0.99 ± 0.9			8.3 ± 3	0.8 ± 1.0	0.10
	May, 15	3	11 ± 3	0.55 ± 0.6	0.93 ± 0.8			4.9 ± 2	0.2 ± 0.2	0.04
	Aug, 15	3	1.9 ± 0.10	0.39 ± 0.03	0.60 ± 0.01	341	2.3	0.6 ± 0.0	0.1 ± 0.0	0.16
Location 2	Feb, 15	1	7.2	2.6	—	39	2.4 ± 0.9	3.0	1.1	0.36
	May, 15	3	10 ± 16	1.10 ± 2	0.14 ± 0.01	132	4.3 ± 1.2	4.6 ± 7.5	0.5 ± 0.8	0.11
	May, 15	3	2.5 ± 2	0.4 ± 0.3	—			1.1 ± 0.8	0.2 ± 0.1	0.18
	May, 15	3	7.9 ± 4	0.18 ± 0.16	0.17 ± 0.00			3.6 ± 2.0	0.1 ± 0.1	0.03
Location 3	Feb, 15	1	25	1.4	—	39.7	5.2 ± 2	4.9	0.3	0.06
Location 4	Aug, 15	3	31 ± 1	1.6 ± 0.5	0.53 ± 0.01	301	3.1 ± 0.6	10.0 ± 0.6	0.5 ± 0.2	0.05
Location 5	Feb, 15	1	14	4.4	15	39	3.9 ± 0.3	3.6	1.1	0.31
Wetland	May, 15	3	0.3 ± 0.10	0.3 ± 0.2	0.56 ± 0.3	76	3.2 ± 0.07	0.1 ± 0.0	0.1 ± 0.1	1.01

[a] Sample collection dates were February 23rd, May 11th, and August 14th of 2015. [b] *N*: number of replicates per plant. [c] Error values were calculated as the standard deviation of the measurements for each sample set. [d] Water and sediments data was published in Blake *et al.* (2017).[4] [e] BF: bioconcentration factor, $BF = \frac{[U]_{root,stem}}{[U]_{sediment}}$. [f] TF: translocation factor, $TF = \frac{[U]_{stem}}{[U]_{root}}$.

multiple pixels to be obtained enabling concentrations of minor elements to be detected much more effectively.

The same root samples analyzed with the STEM were used in JEOL 8200 Electron Microprobe. The microprobe is equipped with 5 wavelength dispersive X-ray spectrometers (WDS) and an ultrathin-window energy dispersive spectrometer, in addition to secondary electron (SE) imaging and backscattered electron (BSE) imaging detectors.

A polished section of the roots was mapped for elemental distribution using the Synchrotron micro-X-Ray Fluorescence (μ-XRF) beam line (BL) 10-2 at the Stanford Synchrotron Radiation Light Source (SSRL). The maps were collected using a Si (111) double crystal monochromator, with an incident angle (ϕ) of 90°, at a 50 μm resolution up to 17 200 eV X-ray energies, just above the U L_{III} edge. All data processing was conducted using the Microanalysis Toolkit software program.

X-ray Absorption Spectroscopy (XAS) measurements were performed at beamline 4-1 at the SSRL. Measurements were done at the U L_3 edge using a double crystal Si(220) monochromator, calibrated at the first inflection point of a Y metal foil absorption at 17 038.4 eV. No change was observed through consecutive scans, nor changes in the absorption when first and last scans of the series, ruling out beam damage during the measurement. Reference spectra for "U(VI) sorbed" corresponds to U(VI) adsorbed to ferrihydrite[71] and uraninite[72] were obtained from previous studies. Uranyl carbonate ("U(VI) carbonate") in the form of andersonite was purchased from the Mineralogical Research Company (San Jose, CA) and the mineralogy was confirmed using X-ray diffraction and XAS. Samples sets were reduced and analyzed using Athena and Artemis[73] with standard methods and benchmarks. Additional details are included in the ESI for shell-by-shell fitting using a similar approach to that used in a previous study.[71]

High-Resolution Transmission Electron Microscope (HR-TEM): after washing thoroughly with 18 MΩ water, small root segments (~5 mm in length) were fixed for 48 h at 4 °C in 2.5% glutaraldehyde prepared in 0.1 M sodium cacodylate buffer (pH = 7.4). Then they were post-fixed for 1 h using 1% osmium tetroxide which was also prepared in 0.1 M sodium cacodylate buffer. After the post fixation, roots were dehydrated in acetone and embedded in resin (Hard Plus Resin-812). Ultrathin sections with nominal thickness ranging from 30 to 70 nm, were cut with an ultramicrotome from the embedded root samples. Samples were analyzed at a LaB_6 Jeol-2100 TEM, operated at 200 keV. The TEM is equipped with a Jeol EX-230 Silicon Drift Detector (SDD) with a 60 mm^2 window of acquisition for the collection of Energy Dispersive X-ray Spectra (EDS) and EDS. STEM digital scanning images were acquired while collecting EDS maps with a JEOL EM-245111SIOD bright field STEM detector.

3. Results and discussion

3.1. Uranium accumulation in plants from the field

Tamarix plants collected from the field accumulated considerable U concentrations (ranging from 10.8–58.9 mg kg^{-1}) in the root system, in spite of the intermittent flow of the Rio Paguate in New Mexico, which limits U transport from the mine. The analysis of acid digested plants collected at various locations along the Rio Paguate, from the Jackpile mine to the wetland area, and four intermediate locations, are shown in Table 1. Uranium accumulation was mainly detected in plant roots, with limited U root-to-shoot translocation, and lower U concentration was detected in plant samples collected away from the mine. Uranium concentration in the roots of plants collected near the mine was as high as 56 mg kg^{-1} in February 2015, with

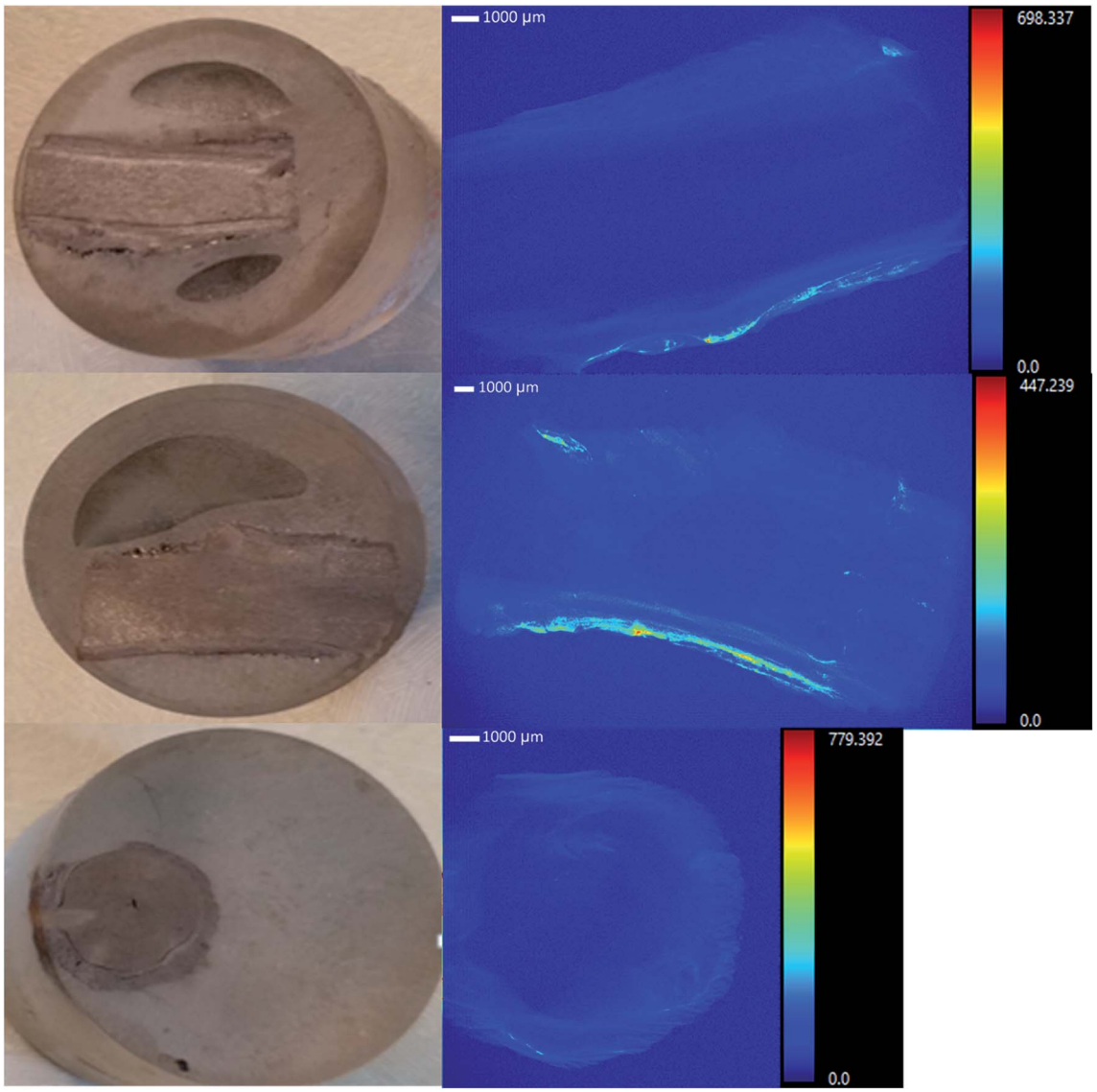

Fig. 1 µXRF studies show that uranium is accumulated in the epidermis and parenchyma cells in the roots from salt cedars collected in the field.

only 1.6 mg kg^{-1} measured in the stem of the plant. However, the concentration of U detected in roots collected downstream from the mine was 25 mg kg^{-1} and 14 mg kg^{-1}, which was 2 to 4-fold lower than that measured close to the mine. Previous work shows that U concentration in river waters ranged between 35.3 to 39.7 µg L^{-1} during the sampling events for this study, and only up to 3 mg kg^{-1} was measured in the sediments.

In samples collected in May 2015, U concentrations were 148 µg L^{-1} in water and 2.2 ± 0.05 mg kg^{-1} in sediments.[4] The concentration of U in the roots of samples collected in May 2015 ranged from 11 ± 3 to 25 ± 5 mg kg^{-1} near the mine, and the concentration in stem and leaves ranged between 0.55 ± 0.6 to 7.3 ± 0.2 mg kg^{-1}. Downstream in the wetland, the concentration of U in the plants was below 1 mg kg^{-1} U, while concentrations of 76 µg L^{-1} U in water and 2.3 ± 0.07 mg kg^{-1} U in sediments were detected. Similarly, in August 2015, 341 µg L^{-1} U was measured in water near the mine, and 1.9 ± 0.10 mg kg^{-1} U was detected in the roots of *Tamarix*. Plant heterogeneity rendered high variability in U content for some samples in the same location, but the U uptake and accumulation by *Tamarix* roots along the Rio Paguate decreased with increasing distance to the Jackpile mine. Selected root samples were analyzed using a synchrotron based micro-X-ray fluorescence (µ-XRF) elemental maps (Fig. 1), and showed U accumulation in the epidermis and parenchyma cells, with little radial transport towards the inside of the root.

The potential of *Tamarix* plants for U phytoaccumulation was evaluated based on the accumulation pattern in the roots and shoots of plants ($N = 31$) collected from the field and in the sediments. The bioconcentration factor (BF), defined as the ratio of U content in plant part to that of sediments, in the roots ranged from 0.1 ± 0.0 to 20.4, with an average of 5.1 ± 5 in the roots, while in the shoots was lower than 1 (average of 0.41 ± 0.5), underlying the potential of *Tamarix* for U bioaccumulation

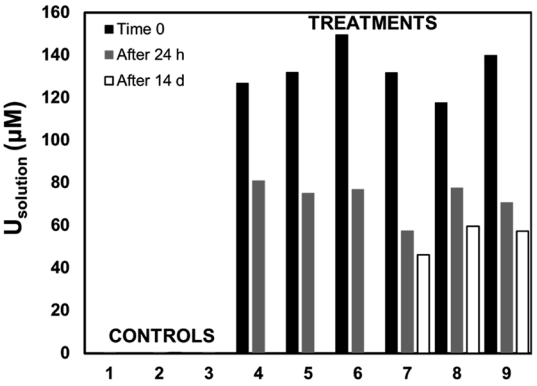

Fig. 2 Uranium concentration in solution in the *in vitro* experiments for controls (samples 1–3) containing 0 μM U, and replicates (samples 4–9) containing 100 μM U. Samples were collected at time zero (full bars), after 24 h of incubation (grey bars), and after 14 d of incubation in controls 1 and 2, and samples 7, 8, and 9 (empty bars).

and to stabilize U mainly in the roots system. These values are much higher than those reported in the literature for native plants growing at the mine sites, which are in the order of 10^{-2} to 10^{-3} in soil plants in a U mine in Portugal,[74] and between 0.051 and 0.234 in native plants in the Sonoran Desert, USA.[75] Interestingly, the high localization of U in the parts of *Tamarix* plants, in particular the roots, was noted along with the presence of low U concentrations in the sediments explaining the relative high BF and underlying the potential of this plants for U accumulation in the roots system along the Rio Paguate. The mean of translocation factor (TF), defined as the ratio of U content in the shoots to that of roots, was found lower than 1 ($TF = 0.26 \pm 0.3$), corresponding to the accumulation and immobilization of U in the roots system. The elucidation of specific mechanisms for U uptake and accumulation of *Tamarix* collected from the field is complicated by our limited knowledge about the age of these plants, the duration and the range of U exposure over the typical seasonal variation of U concentration in water.[4] Additionally, measuring U in plants grown under natural field conditions represents a major challenge since the magnitude of the concentrations encountered is lower than most analytical instruments are capable of detecting. In an attempt to overcome some of these challenges, additional *in vitro* experiments were conducted under laboratory controlled conditions to investigate the mechanisms affecting the interaction between the U and *Tamarix* plant root cells.

3.2. Uranium extracellular precipitation during *in vitro* experiments

Living roots of *Tamarix* collected from the field were exposed to U in *in vitro* experiments in which we observed the decrease of U concentrations in solution, and accumulation of U in these roots. The concentration of U in solution decreased between 36–59% after 24 h, and between 49–65% after two weeks of incubation (Fig. 2). The accumulation of U in the roots exposed to these experiments ranged from 551.4 to 1208.2 mg kg^{-1}. These concentrations are comparable to those reported for U accumulation in plants from other studies.[48,59,60,76] El Hayek *et al.*[60] observed that U uptake by *Brassica juncea* occurred mainly in the first 24 h, and that U uptake followed a pseudo-first order kinetics, in which U uptake is greatly dependent on U concentration in solution. A μ-XRF elemental map of the roots exposed to *in vitro* experiments (Fig. S2 in ESI†) shows a similar profile to that observed for roots collected from the field, with U predominantly accumulating in the epidermis and parenchyma cells. The similar form of accumulation in the external tissues of the root observed in field and laboratory roots validates the purpose of these *in vitro* experiments to evaluate the mechanisms of U uptake by plant roots. Since the roots exposed to *in vitro* experiments accumulated U concentrations in a range (551.4 to 1208.2 mg kg^{-1} U) that could be detectable by microscopic and spectroscopic techniques, further analyses were conducted to investigate U accumulation in cellular structures.

Adsorption of U was confirmed using U-L_{III} XAS analysis (Fig. 3). XANES spectra show that U is present as U(VI). The EXAFS shell-by-shell fitting suggests that U is associated with C functional groups in the plant roots, and it does not show a U–U shell in ~3.85 Å as indicated in other studies, characteristic of uraninite and other microbially-mediated U precipitates.[77] We performed a shell-by-shell fit trying to evaluate the coordination U with P and C shells. The number of atoms for P resulted in a negative number, with the same number of degrees of freedom, therefore discarding the possibility of U–O–P coordination from the EXAFS results. This information is presented in Table S2 in the ESI.† Thus, the U–C coordination is more feasible based on these analyses. It should be noticed that the XAS signal corresponds to the bulk of the sample. Shell fitting parameters are presented in Table 2. Microscopic observations suggest that the accumulation of U in the roots is localized near the vascular region, as the water is transported and distributed through the plant cells. Microscopic imaging with SEM in Fig. 4 shows a U precipitation localized in tracheids near the xylems of the root. A 95× magnification image of the root was obtained with the cortex shown in the top (Fig. 4A). As the magnification increases focusing in the xylems, a precipitate is observed (Fig. 4B, D and E). The EDS of the precipitate confirm the presence of U, as well as C, O, Ca and other minor cations, most likely from the plant tissue (Fig. 4C). This precipitate was found widespread throughout the root section near the xylem. Electron microprobe mapping of the same root used for SEM, but turned 90° (Fig. S3 in the ESI†) shows the general accumulation of U in the endodermis cells near the vascular region following the radial transport of U through the parenchyma cells.

As U is uptaken and transported through the inside of the root, U reacts with chemically functionalized groups in the plant cells, that will increase the local U concentration, allowing the formation of a precipitate, becoming entrapped and immobilized in the cell walls as observed in a TEM image shown in Fig. S3 in the ESI.† The U precipitation might occur by the complexation of U with the carbon (C) in the polysaccharides and pectin groups or with the P phospholipids in the cell membrane.[78–80] Another potential mechanism is the secretion of extracellular phosphate by the phosphatase enzyme to biomineralize U to U–P minerals, which is commonly used as

a heavy metal and U detoxification mechanism by common soil microorganisms[81–84] and by plants,[58,59,85] as heavy metal exposure induces changes in the expression of phosphatase and the production of extracellular and intracellular phosphates.[86,87]

The experimental concentration of 100 μM U in solution at pH 7 was used in this study to assess, in a controlled setting, the effect of elevated U concentrations that could be encountered in the field,[4] awhile allowing the detection of U by spectroscopy and microscopy methods. However, chemical equilibrium calculations using MINEQL 4.6+ suggest that schoepite ($[(UO_2)_4O(OH)_6](H_2O)_6$) precipitation, a uranyl-oxide hydroxyl-hydrate mineral is possible under these experimental conditions. Even if the solution was saturated with respect to a U(VI)–mineral, it is interesting to see that the deposition of U in the roots observed in the *in vitro* experiments (Fig. S2 and S3 in ESI†) is also observed in plant roots collected from the field (Fig. 1). Future experiments are necessary to investigate the accumulation of U in plant roots exposed to different concentrations of U and other environmentally relevant water chemistry conditions. Additional electron microscopy analyses were conducted to analyze in more detail the chemistry and morphology of the U precipitates formed in the plant roots during the *in vitro* experiments.

Table 2 EXAFS fitting parameters for root section exposed to 100 μM U[a]

	U–O1	U–O11	U–C1
N	**2**	**6**	1.8 ± 0.8
D (Å)	1.78 ± 0.01	2.36 ± 0.02	2.87 ± 0.03
σ^2 (Å^2)	0.0016 ± 0.0001	0.012 ± 0.001	**0.004**

[a] *N*: number of scatterers; *D*: distance to the scatterer (Å); σ^2: Debye–Waller factor for each shell (Å^2).

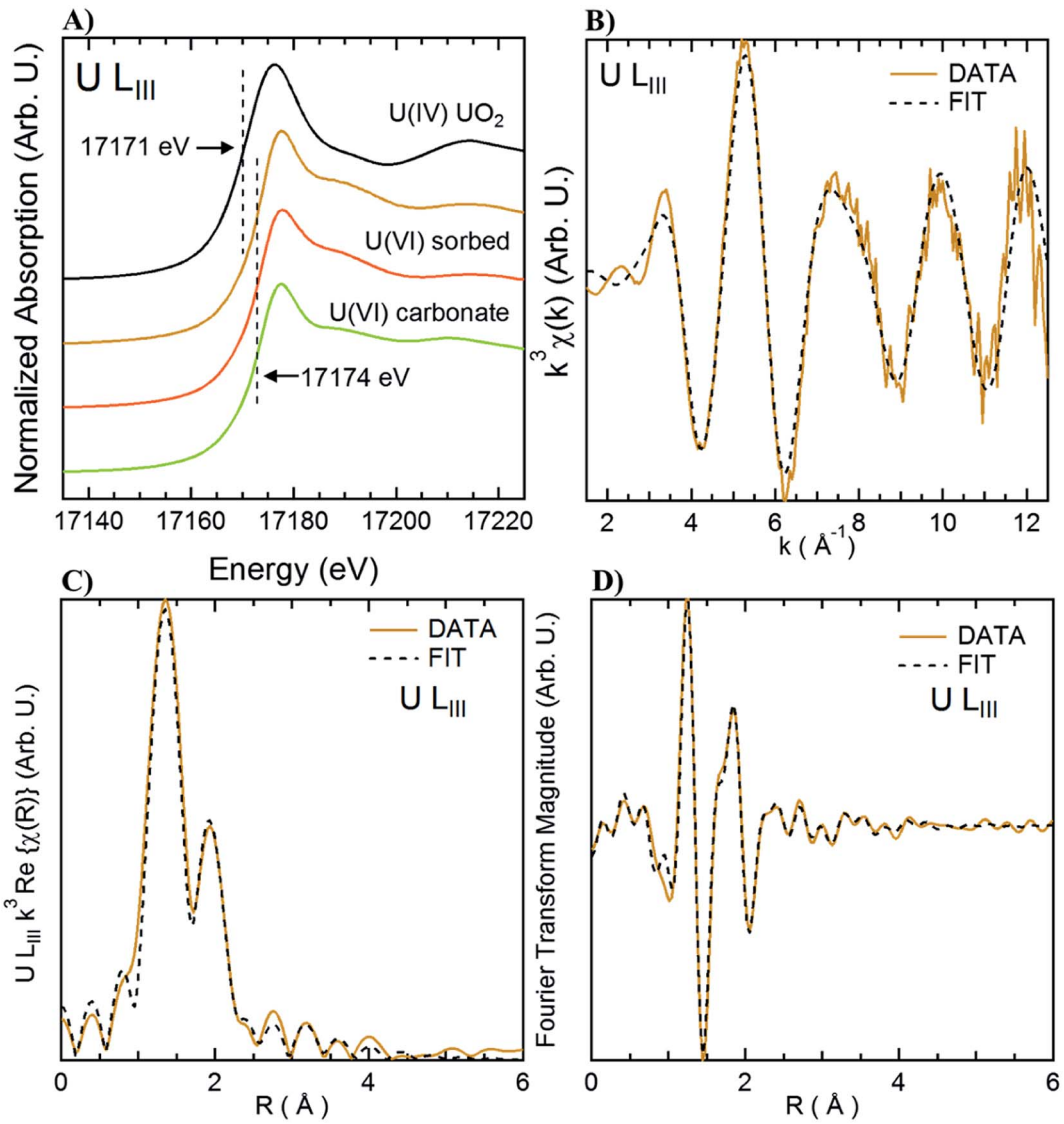

Fig. 3 XAS analysis of root section incubated with 100 μM U. Orange line is the sample spectra. Panel A: U L_{III} XANES spectra; panel B: k3 U L_{III} EXAFS fitting; panel C: shell fitting of the U L_{III} EXAFS spectra; panel D: Fourier Transform fitting. Dashed lines represent the fitted data.

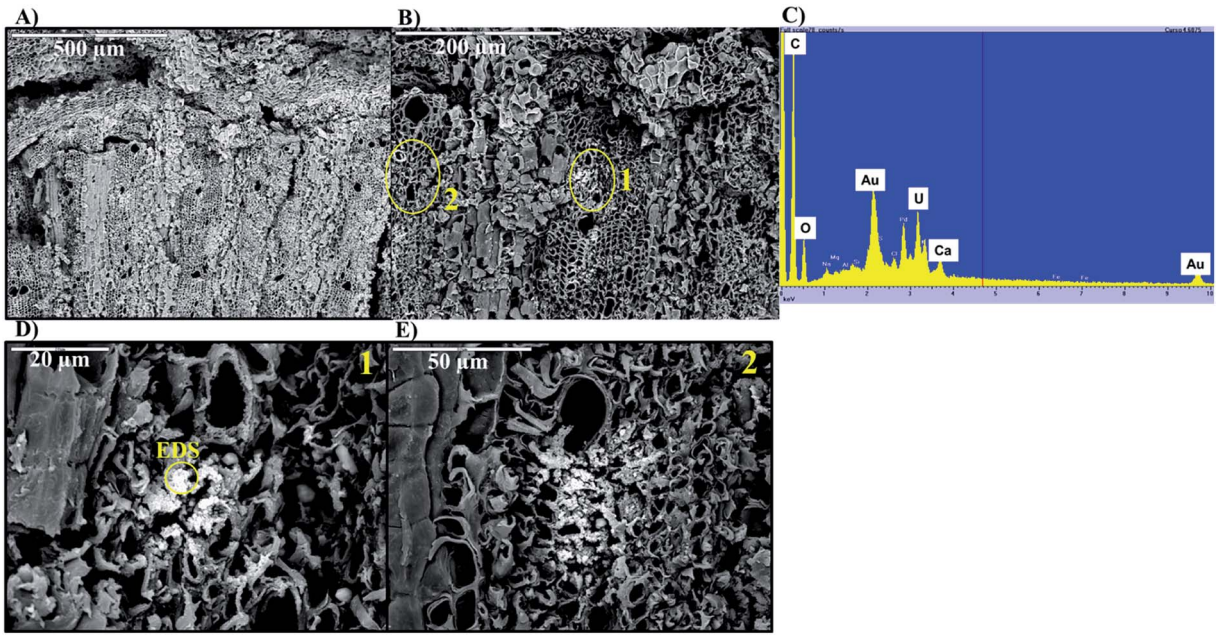

Fig. 4 Formation of U-precipitate inside the roots in SEM images of the root section incubated with 100 μM U for 24 h. Panel A: 95× magnification; panel B: 250× magnification; panel D: 850× magnification of section 1 in panel B; panel E: 850× magnification of section 2 in panel B; and, panel C: EDS of panel E.

3.3. Formation of intracellular U–P nanocrystals during *in vitro* experiments

The mechanisms for accumulation of U in the roots was not only limited to extracellular precipitation to the cell wall or cell membrane. High-resolution TEM images (Fig. 5B and C) of the plant cells show needle-like nanocrystals in vesicles inside the cellular environment. These nanocrystalline structure lengths ranged from less than 30 nm to 300 nm, but the diameters were less than 7 nm. Nanoparticles, less than 30 nm in diameter were commonly associated with the larger prismatic particles and are found dispersed in the surrounding region (Fig. S5 in the ESI†). Electron diffraction patterns could not identify the nature of the crystal, but these particles are mainly made of U, P and O, as

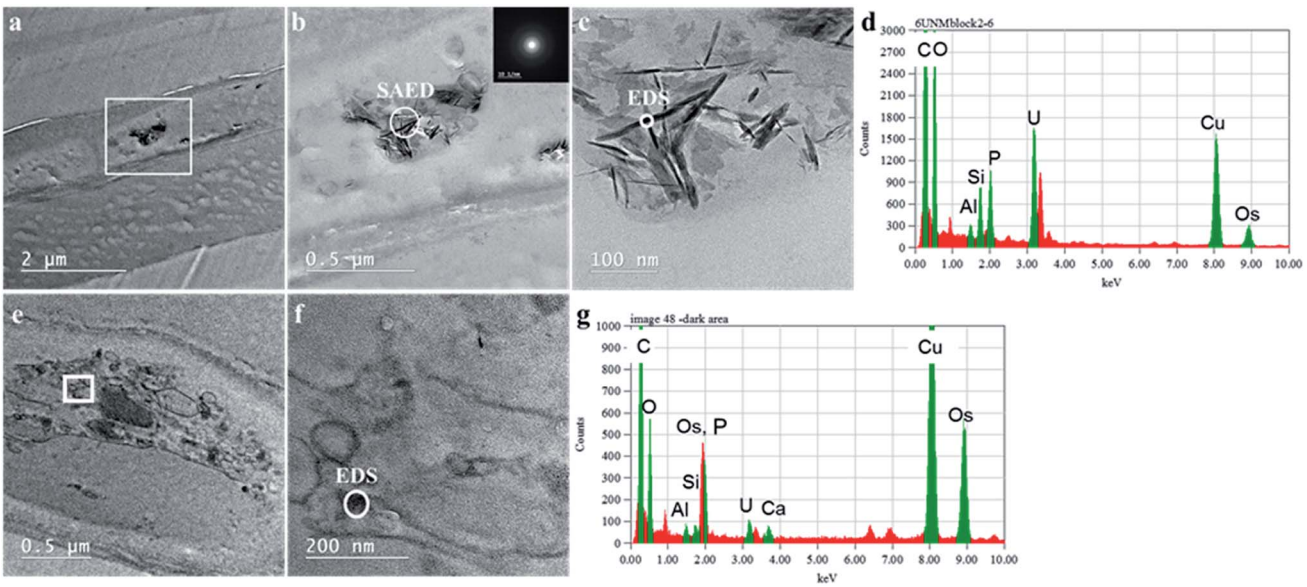

Fig. 5 High resolution TEM of the root section incubated with 100 μM U for 24 h with Energy Dispersive Spectroscopy (EDS). Images in the top row shows a plant root cell with a high-density material in the region inside the square (panel a), with energy diffraction pattern of particles in panel b, EDS of the particles in the panel c shown in panel d. The bottom row show a different conglomerate of cells in panel e, and the EDS of the particles in panel f shown in panel g.

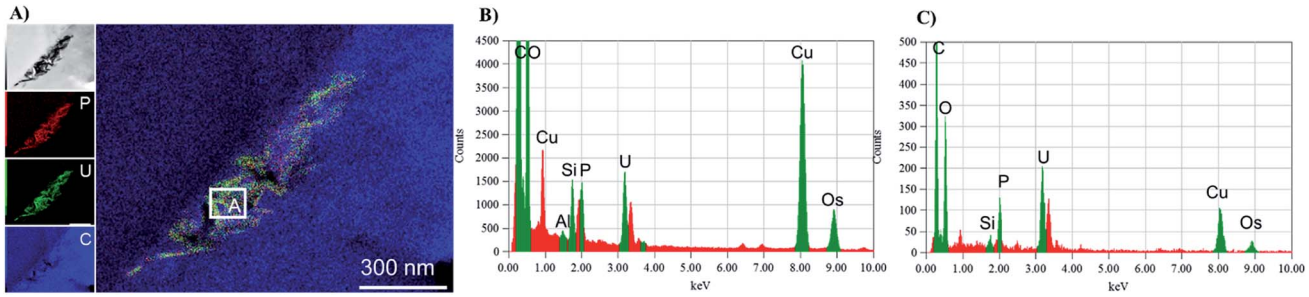

Fig. 6 TEM-EDS mapping of a particle agglomerate (panel A) inside with cumulative EDS of the whole area (panel B) and the EDS from section A in the map (panel C).

presented in the EDS analysis in Fig. 5D and G. A small fraction of K, Al, Si, and other elements are also present (Fig. S6 in the ESI†). The EDS on the surface of these nanocrystals suggests that U is generally found with P. Further characterization of a particle aggregate inside a cell (Fig. 6) confirms the correlation between U and P in these nanoparticles compared to the background EDS signal. The EXAFS fits suggest that U adsorption through U–C coordination occurs in the root sample. This is likely because the bulk of the root material contains abundant organic functional groups that could bind with U. The U–P nanocrystals detected by TEM are discrete, and do not correspond to the bulk of the sample. Thus, the data obtained by XAS and TEM are complementary and indicate that while the bulk of U is adsorbed in the root surface through U–C coordination, there are discrete U–P nanocrystals that were detected by TEM. Hence, U is being uptake and precipitated in a needle-like nanocrystal in the cellular environment.

The formation of these nanoparticles is probably the result of the complexation of U with extracellular phosphate, precipitation of U–P minerals, and the entrapment of the particles inside the cell small vesicle through an endocytic or pinocytotic active transport. Previous studies with oat roots[88] and *Hordeum vulgare* (Barley)[89] exposed to 1 mM to 0.1 mM U concentrations observed the formation of high electron density needle-like nanoparticles accumulated in the cell wall and cell membranes of the plants, with little amorphous material precipitate entrapped in vacuoles in the cells. Most recent studies with cultured water plants (*Spirodela punctata*[90] and *Landoltia punctata*,[59] exposed to 0.2 and 0.4 mM U), laboratory growth *Helianthus annus* (sunflower)[58] (exposed to 0.1 mM U), and hydroponic growth of *Brassica juncea* (exposed to 0.1–2.9 μM U)[60,64] also observed the formation of U-rich nano-crystals accumulated mainly in cell wall and cell membranes, with little U accumulation inside vesicles. Plant detoxification mechanisms for heavy metals focus on preventing cellular uptake promoting binding to the cell wall or cell exudates, and by storage and sequestration of heavy metals into vesicles through cellular transporters.[87,91] Field-grown *Tamarix* roots (this study), when exposed to higher U concentrations, were able to precipitate U–P needle-like nanocrystals and they favor cellular entrapment of U–P nanocrystals over cell wall or cell membrane precipitation, with most of the nanocrystals found in vesicles or vacuoles inside the cells. The greater U cellular entrapment is critical in U stabilization and U immobilization control, and future research must evaluate the U-cellular uptake interaction, toxicity levels, and long-term U accumulation by the root system.

Plants have evolved several mechanisms to tolerate metal toxicity by modulating the intracellular mobility of metal, its reactivity with the cellular components, and root-to-shoot translocation. Such mechanisms determine plant tolerance against metal toxicity, the content and rate of accumulation of metal in the plant, and consequently the mobility and bioavailability of the metal in the environment. The detected insoluble U–P nanocrystals in this study could represent an important role affecting metal solubility in plant cells and, consequently, affecting the rate of U intracellular accumulation, its cellular mobility, and the induced oxidative stress in the plant cell. However, more information is needed to understand the mechanistic processes of U accumulation–precipitation with indigenous P in the plant and how these processes are related to the mechanisms of U toxicity. Furthermore, as U chemotoxic effect has been mainly considered and identified in the literature, little is known if U radiotoxicity also influences the mechanisms of accumulation and detoxification by the plant. The radioactive exposure doses have been studied in the case of other elements with potential radiation activity. For example, Biermans *et al.* reported that plant growth influences the absorbed dose and the dose rate of ^{41}Am (α-radiation), ^{90}Sr (β-radiation) and ^{133}Ba (γ-radiation), and that these doses are strictly depending on the radionuclide element and the organ involved. Future studies should investigate if any relationships exist between the exposure dose rate to uranium, the absorbed dose by the plant organ, and the induced toxicity effects in the plant.

4. Conclusions

We have investigated the mechanisms of U accumulation in *Tamarix* growing along the Rio Paguate near an abandoned U mine, the Jackpile mine. Our results suggest that plants uptake soluble U present in the river. *Tamarix* plants collected from the field showed elevated U concentration in the roots, with limited translocation to the shoots and leaves. *In vitro* experiments with living roots of mature field-grown *Tamarix* were effective to stimulate U uptake by root cells as shown by the similar U

microprobe profile between field and *in vitro* roots and the agreement with previous studies. The *in vitro* studies indicate that, following U uptake by *Tamarix*, as the U is transported through the inside of the root, it reacts and complexes with endogenous elements, potentially C and P in the cell wall and cell membrane or with enzymatic extracellular phosphate. The U complexation increases the local concentration of U reaching saturation, and extracellular precipitation of U occurs. Uranium–P intracellular needle-like nanocrystals are formed and entrapped inside the cell in vesicles. The preferable binding of U to the root cells may explain the retention of U in the roots and thus its weak translocation toward *Tamarix* leaves collected from the field.

The *Tamarix* plants are invasive species to the semi-arid region of the Southwestern United States,[92] consuming considerable water and replacing most of the native vegetation in the infested areas.[93] Several attempts to control the spread of *Tamarix* have been complicated due to the resilience of the plant and their strong root systems.[94] Their extensive root systems, abundance in areas near uranium abandoned mines, and capability to immobilize U in the roots highlight their importance controlling U transport in the area. This work provides a unique perspective of the processes affecting the accumulation of U inside the roots of field-grown plants, which can inform exposure assessment and phytoremediation strategies. Future initiatives could further explore the advantageous use of *Tamarix* for immobilization of U in contaminated sites, in order to prevent U transport and limit exposure of nearby communities. Future research is needed to investigate the maximum uranium accumulation capacity by the plant, and the fate of uranium after plant death to assess the long-term viability of *Tamarix* as U-sink the environment.

Conflicts of interest

There are no conflicts to declare.

Acknowledgements

The authors thank the members of Laguna Pueblo for supporting this work. The authors would like to acknowledge the existing partnership with the Pueblo of Laguna Environment and Natural Resources Department. This work was supported by the National Institute of Health Centers of Excellence on Environmental Health Disparities Research (Grant numbers 1-P50-ES-026102-01 and US-EPA 836157-01), the National Institute of Environmental Health Sciences Superfund Research Program (Award 1-P42-ES-025589), and the National Science Foundation (NM EPSCoR #IIA-1301346 and CAREER 1652619). Part of this work was supported by the Virginia Tech National Center for Earth and Environmental Nanotechnology Infrastructure (NanoEarth), a member of the National Nanotechnology Coordinated Infrastructure (NNCI), supported by the National Science Foundation (ECCS 1542100). Part of this research was carried out at the Stanford Synchrotron Radiation Light source, a national user facility operated by Stanford University on behalf of the US DOE-OBER. The views expressed in this document are solely those of the authors and do not necessarily reflect those of the Agencies.

Notes and references

1 G. H. Fettus and M. G. McKinzie, *Nuclear Fuel's Dirty Beginnings: Environmental Damage and Public Health Risks from Uranium Mining in the American West*, White paper prepared by Natural Resources Defense Council, May 2012.
2 U.S. Department of the Interior, *Abandoned Mine Lands – A New Legacy, Bureau of Land Management*, 2013.
3 International Atomic Energy Agency, *Estimation of Global Inventories of Radioactive Waste and Other Radioactive Materials*, Vienna, 2008.
4 J. M. Blake, C. L. De Vore, S. Avasarala, A.-M. Ali, C. Roldan, F. Bowers, *et al.*, Uranium mobility and accumulation along the Rio Paguate, Jackpile Mine in Laguna Pueblo, NM, *Environ. Sci.: Processes Impacts*, 2017, **19**(4), 605–621.
5 S. R. Taylor, Abundance of chemical elements in the continental crust: a new table, *Geochim. Cosmochim. Acta*, 1964, **28**(8), 1273–1285.
6 National Resources Council, *Uranium mining in Virginia: scientific, technical, environmental, human health and safety, and regulatory aspects of uranium mining and processing in Virginia*, National Academies Press, 2012.
7 J. Lewis, J. Hoover and D. MacKenzie, Mining and Environmental Health Disparities in Native American Communities, *Curr. Environ. Health Rep.*, 2017, **4**(2), 130–141.
8 M. E. Harmon, J. Lewis, C. Miller, J. Hoover, A.-M. S. Ali, C. Shuey, *et al.*, Residential proximity to abandoned uranium mines and serum inflammatory potential in chronically exposed Navajo communities, *J. Exposure Sci. Environ. Epidemiol.*, 2017, **27**(4), 365.
9 L. Newsome, K. Morris and J. R. Lloyd, The biogeochemistry and bioremediation of uranium and other priority radionuclides, *Chem. Geol.*, 2014, **363**, 164–184.
10 J. M. Zachara, P. E. Long, J. Bargar, J. A. Davis, P. Fox, J. K. Fredrickson, *et al.*, Persistence of uranium groundwater plumes: Contrasting mechanisms at two DOE sites in the groundwater–river interaction zone, *J. Contam. Hydrol.*, 2013, **147**, 45–72.
11 J. M. Blake, S. Avasarala, K. Artyushkova, A.-M. S. Ali, A. J. Brearley, C. Shuey, *et al.*, Elevated Concentrations of U and Co-occurring Metals in Abandoned Mine Wastes in a Northeastern Arizona Native American Community, *Environ. Sci. Technol.*, 2015, **49**(14), 8506–8514.
12 J. G. Catalano, J. P. McKinley, J. M. Zachara, S. M. Heald, S. C. Smith and G. E. Brown, Changes in Uranium Speciation through a Depth Sequence of Contaminated Hanford Sediments, *Environ. Sci. Technol.*, 2006, **40**(8), 2517–2524.
13 A. P. Deditius, S. Utsunomiya and R. C. Ewing, The chemical stability of coffinite, USiO4·nH2O; 0< n< 2, associated with organic matter: a case study from Grants uranium region, New Mexico, USA, *Chem. Geol.*, 2008, **251**(1–4), 33–49.

14 J. R. Bargar, R. Reitmeyer and J. A. Davis, Spectroscopic confirmation of uranium (VI)– carbonato adsorption complexes on hematite, *Environ. Sci. Technol.*, 1999, **33**(14), 2481–2484.
15 W. Dong and S. C. Brooks, Determination of the formation constants of ternary complexes of uranyl and carbonate with alkaline earth metals (Mg2+, Ca2+, Sr2+, and Ba2+) using anion exchange method, *Environ. Sci. Technol.*, 2006, **40**(15), 4689–4695.
16 W. A. de Jong, E. Aprà, T. L. Windus, J. A. Nichols, R. J. Harrison, K. E. Gutowski, *et al.*, Complexation of the Carbonate, Nitrate, and Acetate Anions with the Uranyl Dication: Density Functional Studies with Relativistic Effective Core Potentials, *J. Phys. Chem. A*, 2005, **109**(50), 11568–11577.
17 P. G. Allen, D. K. Shuh, J. J. Bucher, N. M. Edelstein, T. Reich, M. A. Denecke, *et al.*, EXAFS Determinations of Uranium Structures: The Uranyl Ion Complexed with Tartaric, Citric, and Malic Acids, *Inorg. Chem.*, 1996, **35**(3), 784–787.
18 S. A. Cumberland, G. Douglas, K. Grice and J. W. Moreau, Uranium mobility in organic matter-rich sediments: a review of geological and geochemical processes, *Earth-Sci. Rev.*, 2016, **159**, 160–185.
19 J. J. Lenhart, S. E. Cabaniss, P. MacCarthy and B. D. Honeyman, Uranium (VI) complexation with citric, humic and fulvic acids, *Radiochim. Acta*, 2000, **88**(6), 345–354.
20 P. S. Nico, B. D. Stewart and S. Fendorf, Incorporation of Oxidized Uranium into Fe (Hydr)oxides during Fe(II) Catalyzed Remineralization, *Environ. Sci. Technol.*, 2009, **43**(19), 7391–7396.
21 M. C. Duff, J. U. Coughlin and D. B. Hunter, Uranium co-precipitation with iron oxide minerals, *Geochim. Cosmochim. Acta*, 2002, **66**(20), 3533–3547.
22 Y. Wang, M. Frutschi, E. Suvorova, V. Phrommavanh, M. Descostes, A. A. A. Osman, *et al.*, Mobile uranium(IV)-bearing colloids in a mining-impacted wetland, *Nat. Commun.*, 2013, **4**, 2942.
23 H. Ching-kuo Daniel and D. Langmuir, Adsorption of uranyl onto ferric oxyhydroxides: Application of the surface complexation site-binding model, *Geochim. Cosmochim. Acta*, 1985, **49**(9), 1931–1941.
24 M. Villalobos, M. A. Trotz and J. O. Leckie, Surface Complexation Modeling of Carbonate Effects on the Adsorption of Cr(VI), Pb(II), and U(VI) on Goethite, *Environ. Sci. Technol.*, 2001, **35**(19), 3849–3856.
25 S. Avasarala, P. C. Lichtner, A.-M. S. Ali, R. González-Pinzón, J. M. Blake and J. M. Cerrato, Reactive Transport of U and V from Abandoned Uranium Mine Wastes, *Environ. Sci. Technol.*, 2017, **51**(21), 12385–12393.
26 W. Dong, T. K. Tokunaga, J. A. Davis and J. Wan, Uranium(VI) Adsorption and Surface Complexation Modeling onto Background Sediments from the F-Area Savannah River Site, *Environ. Sci. Technol.*, 2012, **46**(3), 1565–1571.
27 R. J. Murphy, J. J. Lenhart and B. D. Honeyman, The sorption of thorium (IV) and uranium (VI) to hematite in the presence of natural organic matter, *Colloids Surf., A*, 1999, **157**(1), 47–62.
28 J. R. Bargar, K. H. Williams, K. M. Campbell, P. E. Long, J. E. Stubbs, E. I. Suvorova, *et al.*, Uranium redox transition pathways in acetate-amended sediments, *Proc. Natl. Acad. Sci. U. S. A.*, 2013, **110**(12), 4506–4511.
29 T. Borch, R. Kretzschmar, A. Kappler, P. V. Cappellen, M. Ginder-Vogel, A. Voegelin, *et al.*, Biogeochemical Redox Processes and their Impact on Contaminant Dynamics, *Environ. Sci. Technol.*, 2010, **44**(1), 15–23.
30 B. Gu, L. Liang, M. J. Dickey, X. Yin and S. Dai, Reductive Precipitation of Uranium(VI) by Zero-Valent Iron, *Environ. Sci. Technol.*, 1998, **32**(21), 3366–3373.
31 E. J. O'Loughlin, S. D. Kelly, R. E. Cook, R. Csencsits and K. M. Kemner, Reduction of Uranium(VI) by Mixed Iron(II)/Iron(III) Hydroxide (Green Rust): Formation of UO2 Nanoparticles, *Environ. Sci. Technol.*, 2003, **37**(4), 721–727.
32 V. Noël, K. Boye, J. S. Lezama Pacheco, S. E. Bone, N. Janot, E. Cardarelli, *et al.*, Redox Controls over the Stability of U(IV) in Floodplains of the Upper Colorado River Basin, *Environ. Sci. Technol.*, 2017, **51**(19), 10954–10964.
33 T. A. Robert and D. R. Lovley, *Chapter 7 Microbial redox interactions with uranium: an environmental perspective*, ed. M. J. Keith-Roach and F. R. Livens, Radioactivity in the Environment, Elsevier, 2002, vol. 2, pp. 205–223.
34 M. Ginder-Vogel and S. Fendorf, *Chapter 11 Biogeochemical Uranium Redox Transformations: Potential Oxidants of Uraninite*, ed. M. O. Barnett and D. B. Kent, Developments in Earth and Environmental Sciences, Elsevier, 2007, vol. 7, pp. 293–319.
35 Y. A. Gorby and D. R. Lovley, Enzymic uranium precipitation, *Environ. Sci. Technol.*, 1992, **26**(1), 205–207.
36 D. R. Lovley and E. J. Phillips, Reduction of uranium by Desulfovibrio desulfuricans, *Appl. Environ. Microbiol.*, 1992, **58**(3), 850–856.
37 D. R. Lovley, E. J. P. Phillips, Y. A. Gorby and E. R. Landa, Microbial reduction of uranium, *Nature*, 1991, **350**(6317), 413–416.
38 R. K. Sani, B. M. Peyton, A. Dohnalkova and J. E. Amonette, Reoxidation of Reduced Uranium with Iron(III) (Hydr)Oxides under Sulfate-Reducing Conditions, *Environ. Sci. Technol.*, 2005, **39**(7), 2059–2066.
39 N. F. Spycher, M. Issarangkun, B. D. Stewart, S. Sevinç Şengör, E. Belding, T. R. Ginn, *et al.*, Biogenic uraninite precipitation and its reoxidation by iron(III) (hydr)oxides: A reaction modeling approach, *Geochim. Cosmochim. Acta*, 2011, **75**(16), 4426–4440.
40 H. R. Beller, Anaerobic, nitrate-dependent oxidation of U(IV) oxide minerals by the chemolithoautotrophic bacterium Thiobacillus denitrificans, *Appl. Environ. Microbiol.*, 2005, **71**(4), 2170–2174.
41 J. M. Senko, Y. Mohamed, T. A. Dewers and L. R. Krumholz, Role for Fe(III) Minerals in Nitrate-Dependent Microbial U(IV) Oxidation, *Environ. Sci. Technol.*, 2005, **39**(8), 2529–2536.
42 M.-N. Croteau, C. C. Fuller, D. J. Cain, K. M. Campbell and G. Aiken, Biogeochemical Controls of Uranium

Bioavailability from the Dissolved Phase in Natural Freshwaters, *Environ. Sci. Technol.*, 2016, **50**(15), 8120–8127.
43 L. Du, X. Feng, Z. Huang, B. Liu, Y. Jin, Z. Fang, *et al.*, The effect of U speciation in cultivation solution on the uptake of U by variant Sedum alfredii, *Environ. Sci. Pollut. Res.*, 2016, **23**(10), 9964–9971.
44 S. E. Crawford and K. Liber, Effects of clay minerals and organic matter in formulated sediments on the bioavailability of sediment-associated uranium to the freshwater midge, Chironomus dilutus, *Sci. Total Environ.*, 2015, **532**, 821–830.
45 J. Pratas, P. J. Favas, C. Paulo, N. Rodrigues and M. Prasad, Uranium accumulation by aquatic plants from uranium-contaminated water in Central Portugal, *Int. J. Phytorem.*, 2012, **14**(3), 221–234.
46 V. N. Jha, R. M. Tripathi, N. K. Sethy and S. K. Sahoo, Uptake of uranium by aquatic plants growing in fresh water ecosystem around uranium mill tailings pond at Jaduguda, India, *Sci. Total Environ.*, 2016, **539**, 175–184.
47 A. Boghi, T. Roose and G. J. D. Kirk, A Model of Uranium Uptake by Plant Roots Allowing for Root-Induced Changes in the soil, *Environ. Sci. Technol.*, 2018, **52**(6), 3536–3545.
48 I. Shtangeeva, Uptake of uranium and thorium by native and cultivated plants, *J. Environ. Radioact.*, 2010, **101**(6), 458–463.
49 P. Chang, K.-W. Kim, S. Yoshida and S.-Y. Kim, Uranium Accumulation of Crop Plants Enhanced by Citric Acid, *Environ. Geochem. Health*, 2005, **27**(5), 529–538.
50 M. D. Stojanović, M. L. Mihajlović, J. V. Milojković, Z. R. Lopičić, M. Adamović and S. Stanković, Efficient phytoremediation of uranium mine tailings by tobacco, *Environ. Chem. Lett.*, 2012, **10**(4), 377–381.
51 J. Mihalík, P. Henner, S. Frelon, V. Camilleri and L. Février, Citrate assisted phytoextraction of uranium by sunflowers: Study of fluxes in soils and plants and resulting intra-planta distribution of Fe and U, *Environ. Exp. Bot.*, 2012, **77**, 249–258.
52 P. Malaviya and A. Singh, Phytoremediation Strategies for Remediation of Uranium-Contaminated Environments: A Review, *Crit. Rev. Environ. Sci. Technol.*, 2012, **42**(24), 2575–2647.
53 Y. Wang, A. Bagnoud, E. Suvorova, E. McGivney, L. Chesaux, V. Phrommavanh, *et al.*, Geochemical control on uranium (IV) mobility in a mining-impacted wetland, *Environ. Sci. Technol.*, 2014, **48**(17), 10062–10070.
54 D. I. Kaplan, R. Kukkadapu, J. C. Seaman, B. W. Arey, A. C. Dohnalkova, S. Buettner, *et al.*, Iron mineralogy and uranium-binding environment in the rhizosphere of a wetland soil, *Sci. Total Environ.*, 2016, **569**, 53–64.
55 D. Li, D. I. Kaplan, H.-S. Chang, J. C. Seaman, P. R. Jaffé, P. Koster van Groos, *et al.*, Spectroscopic evidence of uranium immobilization in acidic wetlands by natural organic matter and plant roots, *Environ. Sci. Technol.*, 2015, **49**(5), 2823–2832.
56 N. Edayilam, D. Montgomery, B. Ferguson, A. S. Maroli, N. Martinez, B. A. Powell, *et al.*, Phosphorus Stress-Induced Changes in Plant Root Exudation Could Potentially Facilitate Uranium Mobilization from Stable Mineral Forms, *Environ. Sci. Technol.*, 2018, **52**(14), 7652–7662.
57 J. Laurette, C. Larue, C. Mariet, F. Brisset, H. Khodja, J. Bourguignon, *et al.*, Influence of uranium speciation on its accumulation and translocation in three plant species: Oilseed rape, sunflower and wheat, *Environ. Exp. Bot.*, 2012, **77**, 96–107.
58 J. Laurette, C. Larue, I. Llorens, D. Jaillard, P.-H. Jouneau, J. Bourguignon, *et al.*, Speciation of uranium in plants upon root accumulation and root-to-shoot translocation: A XAS and TEM study, *Environ. Exp. Bot.*, 2012, **77**, 87–95.
59 X. Nie, F. Dong, L. Bian, M. Liu, C. Ding, H. He, *et al.*, Uranium Binding on Landoltia punctata as a Result of Formation of Insoluble Nano-U (VI) and U (IV) Phosphate Minerals, *ACS Sustainable Chem. Eng.*, 2017, **5**(2), 1494–1502.
60 E. El Hayek, C. Torres, L. Rodriguez-Freire, J. M. Blake, C. L. De Vore, A. J. Brearley, *et al.*, Effect of Calcium on the Bioavailability of Dissolved Uranium(VI) in Plant Roots under Circumneutral pH, *Environ. Sci. Technol.*, 2018, **52**(22), 13089–13098.
61 J. M. Di Tomaso, Impact, biology, and ecology of saltcedar (Tamarix spp.) in the southwestern United States, *Weed Technol.*, 1998, 326–336.
62 T. L. Dudley and C. J. Deloach, Saltcedar (Tamarix spp.), endangered species, and biological weed control—can they mix?, *Weed Technol.*, 2004, **18**(sp1), 1542–1551.
63 E. Grijalva, *A Tale of Three Species Invasive species control and endangered species management in the Southwestern US, Saltcedar, leaf beetles and the Southwestern willow flycatcher*, 2015.
64 E. El Hayek, A. J. Brearley, T. Howard, P. Hudson, C. Torres, M. N. Spilde, *et al.*, Calcium in Carbonate Water Facilitates the Transport of U(VI) in Brassica juncea Roots and Enables Root-to-Shoot Translocation, *ACS Earth Space Chem.*, 2019, **3**(10), 2190–2196.
65 E. Steudle, Water uptake by roots: effects of water deficit, *J. Exp. Bot.*, 2000, **51**(350), 1531–1542.
66 H. Küpper, A. Mijovilovich, W. Meyer-Klaucke and P. M. H. Kroneck, Tissue- and Age-Dependent Differences in the Complexation of Cadmium and Zinc in the Cadmium/Zinc Hyperaccumulator *Thlaspi caerulescens* (Ganges Ecotype) Revealed by X-Ray Absorption Spectroscopy, *Plant Physiol.*, 2004, **134**(2), 748–757.
67 W.-M. Xiao, M.-C. Zhao, M. Zou, Y.-D. Tan and X.-G. Zhang, Differences in differential gene expression between young and mature *Arabidopsis* C58 tumours, *Plant Biol.*, 2014, **16**(3), 539–549.
68 A. C. d. S. C. Branco, Vegetative Propagation by Root Cuttings, *Nature*, 1951, **168**(4264), 125–126.
69 B. Ottosson and N. T. Welander, Transpiration rate in relation to root and leaf growth in cuttings of Begonia X hiemalis Fotsch, *Sci. Hortic.*, 1997, **68**(1), 125–136.
70 W. Schecher, *MINEQL DM, A Chemical Equilibrium Modeling System, Version 4.6, 4.5. Environmental Research Software*, Hallowell, ME, 2007.
71 M. S. Massey, J. S. Lezama-Pacheco, M. E. Jones, E. S. Ilton, J. M. Cerrato, J. R. Bargar, *et al.*, Competing retention

pathways of uranium upon reaction with Fe(II), *Geochim. Cosmochim. Acta*, 2014, **142**, 166–185.
72 E. J. Schofield, H. Veeramani, J. O. Sharp, E. Suvorova, R. Bernier-Latmani, A. Mehta, *et al.*, Structure of Biogenic Uraninite Produced by *Shewanella oneidensis* Strain MR-1, *Environ. Sci. Technol.*, 2008, **42**(21), 7898–7904.
73 B. Ravel and M. Newville, ATHENA, ARTEMIS, HEPHAESTUS: data analysis for X-ray absorption spectroscopy using IFEFFIT, *J. Synchrotron Radiat.*, 2005, **12**(4), 537–541.
74 P. J. C. Favas, J. Pratas, S. Mitra, S. K. Sarkar and P. Venkatachalam, Biogeochemistry of uranium in the soil-plant and water-plant systems in an old uranium mine, *Sci. Total Environ.*, 2016, **568**, 350–368.
75 R. Wetle, B. Bensko-Tarsitano, K. Johnson, K. G. Sweat and T. Cahill, Uptake of uranium into desert plants in an abandoned uranium mine and its implications for phytostabilization strategies, *J. Environ. Radioact.*, 2020, **220–221**, 106293.
76 A. D. Butler, M. Wynter, V. F. Medina and A. J. Bednar, Depleted Uranium Toxicity, Accumulation, and Uptake in *Cynodon dactylon* (Bermuda) and *Aristida purpurea* (Purple Threeawn), *Bull. Environ. Contam. Toxicol.*, 2016, **96**(6), 714–719.
77 R. Bernier-Latmani, H. Veeramani, E. D. Vecchia, P. Junier, J. S. Lezama-Pacheco, E. I. Suvorova, *et al.*, Non-uraninite Products of Microbial U(VI) Reduction, *Environ. Sci. Technol.*, 2010, **44**(24), 9456–9462.
78 F. Morcillo, M. T. González-Muñoz, T. Reitz, M. E. Romero-González, J. M. Arias and M. L. Merroun, Biosorption and Biomineralization of U(VI) by the Marine Bacterium *Idiomarina loihiensis* MAH1: Effect of Background Electrolyte and pH, *PLoS One*, 2014, **9**(3), e91305.
79 M. P. Thorgersen, W. A. Lancaster, L. Rajeev, X. Ge, B. J. Vaccaro, F. L. Poole, *et al.*, A Highly Expressed High-Molecular-Weight S-Layer Complex of *Pelosinus* sp. Strain UFO1 Binds Uranium, *Appl. Environ. Microbiol.*, 2017, **83**(4), e03044-16.
80 M. L. Merroun, J. Raff, A. Rossberg, C. Hennig, T. Reich and S. Selenska-Pobell, Complexation of Uranium by Cells and S-Layer Sheets of *Bacillus sphaericus* JG-A12, *Appl. Environ. Microbiol.*, 2005, **71**(9), 5532–5543.
81 L. Macaskie, K. Bonthrone and D. Rouch, Phosphatase-mediated heavy metal accumulation by a *Citrobacter* sp. and related enterobacteria, *FEMS Microbiol. Lett.*, 1994, **121**(2), 141–146.
82 L. E. Macaskie, K. M. Bonthrone, P. Yong and D. T. Goddard, Enzymically mediated bioprecipitation of uranium by a *Citrobacter* sp.: a concerted role for exocellular lipopolysaccharide and associated phosphatase in biomineral formation, *Microbiology*, 2000, **146**(8), 1855–1867.
83 K. S. Nilgiriwala, A. Alahari, A. S. Rao and S. K. Apte, Cloning and overexpression of alkaline phosphatase PhoK from *Sphingomonas* sp. strain BSAR-1 for bioprecipitation of uranium from alkaline solutions, *Appl. Environ. Microbiol.*, 2008, **74**(17), 5516–5523.
84 M. C. Yung and Y. Jiao, Biomineralization of uranium by PhoY phosphatase activity aids cell survival in Caulobacter crescentus, *Appl. Environ. Microbiol.*, 2014, **80**(16), 4795–4804.
85 F. Vera Tomé, P. Blanco Rodríguez and J. C. Lozano, Elimination of natural uranium and 226Ra from contaminated waters by rhizofiltration using Helianthus annuus L., *Sci. Total Environ.*, 2008, **393**(2), 351–357.
86 S. M. G. Duff, G. Sarath and W. C. Plaxton, The role of acid phosphatases in plant phosphorus metabolism, *Physiol. Plant.*, 1994, **90**(4), 791–800.
87 S. Singh, P. Parihar, R. Singh, V. P. Singh and S. M. Prasad, Heavy Metal Tolerance in Plants: Role of Transcriptomics, Proteomics, Metabolomics, and Ionomics, *Front. Plant Sci.*, 2016, **6**, 1143.
88 H. Wheeler and P. Hanchey, Pinocytosis and Membrane Dilation in Uranyl-Treated Plant Roots, *Science*, 1971, **171**(3966), 68–71.
89 A. Robards and M. E. Robb, Uptake and binding of uranyl ions by barley roots, *Science*, 1972, **178**(4064), 980–982.
90 X. Nie, F. Dong, N. Liu, M. Liu, D. Zhang, W. Kang, *et al.*, Subcellular distribution of uranium in the roots of *Spirodela punctata* and surface interactions, *Appl. Surf. Sci.*, 2015, **347**, 122–130.
91 M. K. Hasan, Y. Cheng, M. K. Kanwar, X.-Y. Chu, G. J. Ahammed and Z.-Y. Qi, Responses of Plant Proteins to Heavy Metal Stress—A Review, *Front. Plant Sci.*, 2017, **8**, 1492.
92 J. F. Gaskin and B. A. Schaal, Hybrid *Tamarix* widespread in U.S. invasion and undetected in native Asian range, *Proc. Natl. Acad. Sci. U. S. A.*, 2002, **99**(17), 11256–11259.
93 T. W. Robinson, *Introduction, spread, and areal extent of saltcedar (Tamarix) in the Western States*, 1965, Report No.: 491A.
94 P. B. Shafroth, J. R. Cleverly, T. L. Dudley, J. P. Taylor, C. Van Riper, E. P. Weeks, *et al.*, Control of *Tamarix* in the Western United States: Implications for Water Salvage, Wildlife Use, and Riparian Restoration, *Environ. Manage.*, 2005, **35**(3), 231–246.
95 D. Ribera, F. Labrot, G. Tisnerat and J.-F. Narbonne, Uranium in the Environment: Occurrence, Transfer, and Biological Effects, *Reviews of Environmental Contamination and Toxicology*, Springer New York, New York, NY, 1996, pp. 53–89.
96 T. Mathews, K. Beaugelin-Seiller, J. Garnier-Laplace, R. Gilbin, C. Adam and C. Della-Vedova, A Probabilistic Assessment of the Chemical and Radiological Risks of Chronic Exposure to Uranium in Freshwater Ecosystems, *Environ. Sci. Technol.*, 2009, **43**(17), 6684–6690.